Title

TAOK2 Kinase Mediates PSD95 Stability and Dendritic Spine Maturation through Septin7 Phosphorylation

Journal

Neuron, 93(2)

ISSN

0896-6273

Authors

Yadav, Smita
Oses-Prieto, Juan A
Peters, Christian J
et al.

Publication Date

2017

DOI

10.1016/j.neuron.2016.12.006

Peer reviewed

Article

Neuron

TAOK2 Kinase Mediates PSD95 Stability and Dendritic Spine Maturation through Septin7 Phosphorylation

Highlights

- TAOK2 is required for spine maturation and postsynaptic Ca^{+2} compartmentalization
- TAOK2 phosphorylates the cytoskeletal GTPase Sept7 at the conserved residue T426
- Sept7 phosphorylation at T426 by TAOK2 is required for dendritic spine maturation
- Phosphorylated Sept7 associates with and stabilizes PSD95 promoting spine maturation

Authors

Smita Yadav, Juan A. Oses-Prieto, Christian J. Peters, ..., Alma L. Burlingame, Lily Y. Jan, Yuh-Nung Jan

Correspondence

yuhnung.jan@ucsf.edu

In Brief

Abnormalities in dendritic spines are manifestations of several neurodevelopmental diseases. Yadav et al. show that the serine/threonine kinase TAOK2 is required for dendritic spine maturation and identify the cytoskeletal GTPase Septin7 as its substrate that stabilizes the scaffolding protein PSD95 in spines.

Yadav et al., 2017, Neuron *93*, 379–393
January 18, 2017
http://dx.doi.org/10.1016/j.neuron.2016.12.006

CellPress

Neuron
Article

TAOK2 Kinase Mediates PSD95 Stability and Dendritic Spine Maturation through Septin7 Phosphorylation

Smita Yadav,[1] Juan A. Oses-Prieto,[2] Christian J. Peters,[1] Jing Zhou,[3] Samuel J. Pleasure,[3] Alma L. Burlingame,[2] Lily Y. Jan,[1] and Yuh-Nung Jan[1,4,*]
[1]Departments of Physiology, Biochemistry, and Biophysics, Howard Hughes Medical Institute, University of California, San Francisco, San Francisco, CA 94158, USA
[2]Mass Spectrometry Facility, Department of Pharmaceutical Chemistry, University of California, San Francisco, San Francisco, CA 94158, USA
[3]Department of Neurology, Programs in Neuroscience and Developmental Biology, Institute for Regenerative Medicine, University of California, San Francisco, San Francisco, CA 94158, USA
[4]Lead Contact
*Correspondence: yuhnung.jan@ucsf.edu
http://dx.doi.org/10.1016/j.neuron.2016.12.006

SUMMARY

Abnormalities in dendritic spines are manifestations of several neurodevelopmental and psychiatric diseases. *TAOK2* is one of the genes in the 16p11.2 locus, copy number variations of which are associated with autism and schizophrenia. Here, we show that the kinase activity of the serine/threonine kinase encoded by *TAOK2* is required for spine maturation. TAOK2 depletion results in unstable dendritic protrusions, mislocalized shaft-synapses, and loss of compartmentalization of NMDA receptor-mediated calcium influx. Using chemical-genetics and mass spectrometry, we identified several TAOK2 phosphorylation targets. We show that TAOK2 directly phosphorylates the cytoskeletal GTPase Septin7, at an evolutionary conserved residue. This phosphorylation induces translocation of Septin7 to the spine, where it associates with and stabilizes the scaffolding protein PSD95, promoting dendritic spine maturation. This study provides a mechanistic basis for postsynaptic stability and compartmentalization via TAOK2-Sept7 signaling, with implications toward understanding the potential role of TAOK2 in neurological deficits associated with the 16p11.2 region.

INTRODUCTION

Dendritic spines are the recipient sites for most excitatory transmission. By assembling a complex machinery of scaffolding proteins and glutamate receptors into a biochemically insulated compartment, dendritic spines enable precise synaptic transmission with controlled relay to downstream signaling cascades (Adrian et al., 2014; Blanpied and Ehlers, 2004; Chen and Sabatini, 2012; Colgan and Yasuda, 2014). Spines exhibit diverse structural and functional changes during development, and in learning and memory formation (Hering and Sheng, 2001; Holtmaat and Svoboda, 2009; Nimchinsky et al., 2002; Sala and Segal, 2014), and aberrations in spines are one of the strongest structural correlates of neurodevelopmental and psychiatric diseases involving perturbations in cognition and information processing (Glantz and Lewis, 2000; Hutsler and Zhang, 2010; Irwin et al., 2001; Kaufmann and Moser, 2000; Lin and Koleske, 2010; Penzes et al., 2011). Genetic studies of gene variants and copy number variations have implicated a number of genes associated with neurodevelopmental and psychiatric diseases, many of which converge on pathways regulating dendritic spine and synapse structure (De Rubeis et al., 2014; Pinto et al., 2014; Sebat et al., 2007).

Thousand and one amino acid kinase 2 (TAOK2) encodes a serine/threonine kinase (Moore et al., 2000) and is one of the 29 genes present at the 16p11.2 genomic locus (Weiss et al., 2008). Deletion of this region is the most common genetic risk factor associated with autism spectrum disorder (ASD) accounting for approximately 1% of ASD patients (Kumar et al., 2008; Weiss et al., 2008). Duplication of this region is associated with schizophrenia (McCarthy et al., 2009), underscoring the contribution of abnormal gene dosage toward diverse neurological phenotypes. Changes in TAOK2 gene expression have the highest correlation with head circumference in ASD patients with 16p11.2 copy number variations (CNVs) as compared to other genes in the locus (Luo et al., 2012). Additionally, TAOK2 expression in the human brain is high during early development and is regulated by FMRP, making it a high probability CNV-associated disease relevant gene (Darnell et al., 2011). In mice, disruption of TAOK2 induces defects in basal dendritic growth and agenesis of the corpus callosum (de Anda et al., 2012), and phosphorylation of TAOK2 by the hippo kinase homolog MST3 is required for dendritic spine formation in hippocampal neurons (Ultanir et al., 2014).

Given its relevance in neuronal development and to ASD, it is important to investigate how TAOK2 affects dendritic spine formation and to identify its physiological neuronal substrates. Here, we report that TAOK2 localizes to dendritic spines of hippocampal neurons, and its kinase activity is required for

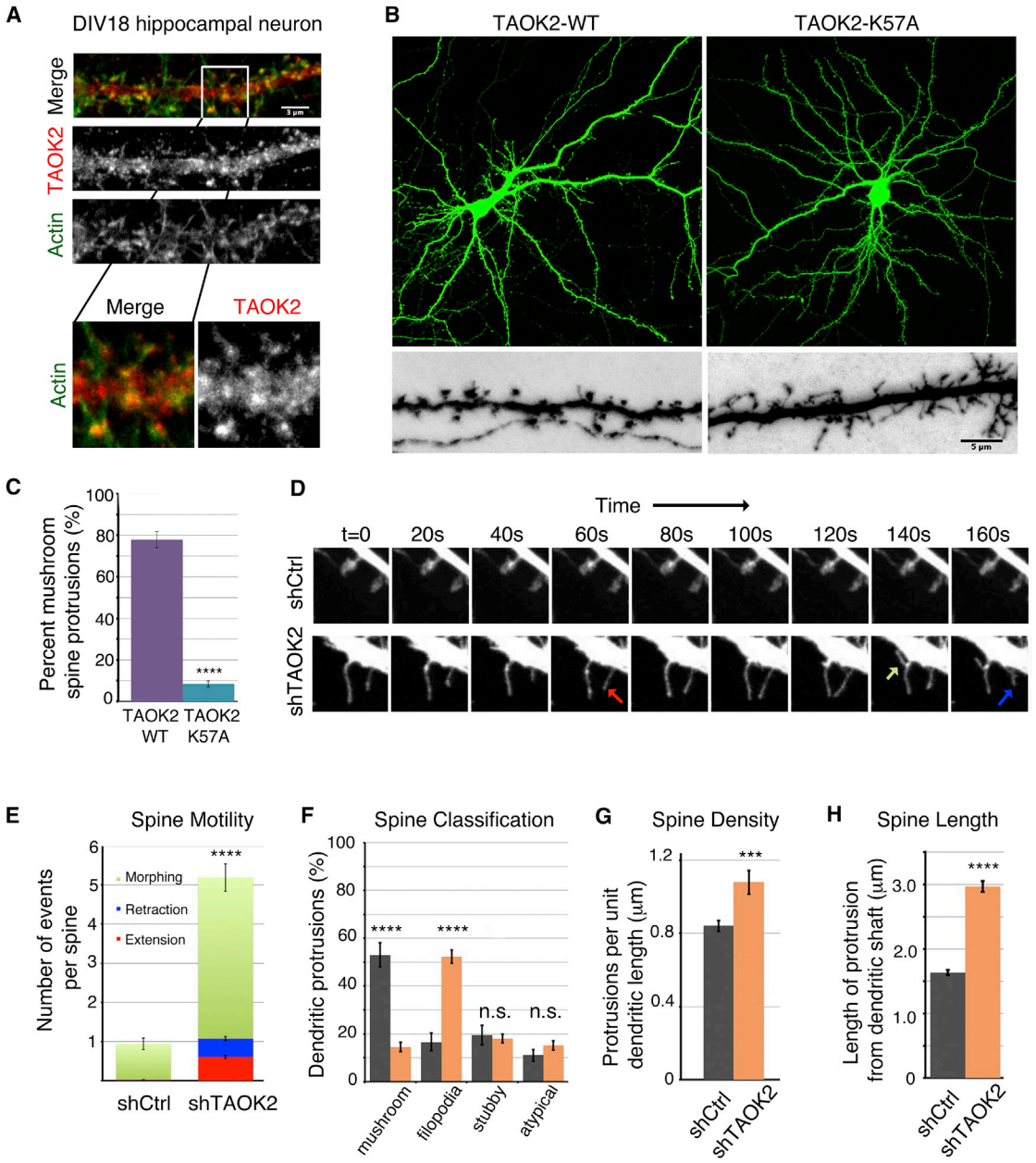

Figure 1. TAOK2 Localizes to Dendritic Spines and Its Kinase Activity Is Required for Spine Maturation

(A) Representative immunofluorescence image of a DIV18 hippocampal neuron stained using an antibody against TAOK2 and Phalloidin to visualize F-actin in dendritic shaft and spines. Magnification of the boxed area (white) is shown below. The scale bar represents 3 μm.

(B) Hippocampal neurons transfected with either human TAOK2-WT (left) or TAOK2-K57A (right) along with EGFP to visualize morphology of dendritic spines. The lower images are higher magnification images. The scale bar represents 5 μm.

(C) Bar graph depicts percent of mature mushroom spine-shaped dendritic protrusions in TAOK2-WT and TAOK2-K57A transfected neurons, respectively (n = 15 per condition, $p < 0.0001$, and t test).

(D) Montage of time-lapse images depicting spine dynamics was created by confocal imaging of dendritic spines of neurons transfected with either control shRNA or shRNA against TAOK2. The green arrow marks a morphing event, the blue arrow marks retraction, and the red arrow marks an extension event.

(E) Number of morphing (green), extension (red), and retraction (blue) events per spine in neurons transfected with either control or TAOK2 shRNA. The five movies from independent experiments were analyzed with at least ten spines per experiment in each condition.

(F) Spine morphology of control and TAOK2 shRNA treated neurons quantified as a percent of total protrusions binned into spine, filopodia, stubby, or atypical protrusions (n = 15 per condition, $p < 0.0001$, and multiple t tests).

(legend continued on next page)

maturation of dendritic spines. TAOK2 knockdown leads to unstable dendritic protrusions and mislocalization of postsynaptic proteins including AMPA receptors to the dendritic shaft, causing synapses to form directly on the dendritic shaft and resulting in loss of compartmentalization of NMDA receptor-mediated calcium influx. Engineering an ATP analog-sensitive TAOK2 kinase allowed us to identify direct substrates of TAOK2 and to determine their phosphorylation sites through chemical genetics and mass spectrometry. Our study reveals novel TAOK2 phosphorylation targets implicated in diverse processes including synaptogenesis, dendrite branching, axon growth, ciliogenesis, and regulation of actin and microtubule dynamics. Our in vivo phosphomutant analyses of the identified candidate substrates and in vitro biochemical kinase assays further show that septin7 (Sept7) is a direct substrate of TAOK2 essential for the maturation of dendritic spines. Expression of phosphomutant Sept7 leads to shaft synapses and deficit in NMDA receptor-mediated calcium compartmentalization. Moreover, TAOK2 mediated Sept7 phosphorylation is required for spine stability through a phosphorylation-dependent interaction of Sept7 with the postsynaptic scaffolding protein PSD95. This study reveals how TAOK2 kinase activity can induce dramatic changes in the dendritic spine and synapse structure, by regulating interaction of the postsynaptic scaffolding machinery with the septin cytoskeleton.

RESULTS

TAOK2 Localizes to Dendritic Spines, and Its Kinase Activity Is Required for Spine Maturation

Alternative splicing results in two TAOK2 isoforms, TAO2α (140 kDa) and TAO2β (120 kDa), that share a conserved N-terminal kinase domain, but differ in their C terminus (Moore et al., 2000; Yasuda et al., 2007). Our immunofluorescence analysis using an antibody that recognizes both isoforms of TAOK2 revealed that, in mature DIV18 hippocampal neurons, TAOK2 was present throughout the neuronal cytoplasm and also localized to the actin-rich dendritic spines and dendritic shaft (Figures 1A and S1A). To explore the functional requirement of the kinase activity of TAOK2 in dendritic spine formation, we tested whether expression of the kinase-dead mutant TAOK2 would affect the spine morphology. In contrast to neurons expressing wild-type TAOK2^{WT}, expression of the kinase-dead mutant TAOK2^{K57A} led to a significant loss of mature mushroom-shaped spines and an increase in the number of immature filopodial protrusions (Figures 1B and 1C). The phenotypic similarity of the filopodial protrusions in neurons expressing kinase-dead TAOK2 to those caused by small hairpin (sh)RNA mediated knock down of TAOK2 (Ultanir et al., 2014) (Figure S1A) is suggestive that TAOK2 mediates spine maturation through its kinase activity.

Confocal live imaging of mature DIV18 hippocampal neurons revealed that, while dendritic spines in control treated neurons were stable and mushroom-shaped, TAOK2 knockdown neurons had highly motile filopodia that underwent rapid extension, retraction, and morphing events. The number of events per spine over a period of 10 min increased from less than one event/spine to greater than five events/spine in neurons transfected with TAOK2 shRNA (Figures 1D and 1E; Movie S1). There was a dramatic increase in immature filopodial protrusions, such that both the density and average length of dendritic protrusions increased with TAOK2 knockdown (Figures 1F–1H). We further performed in utero electroporation of TAOK2 shRNA in mouse embryos (Figures S1C and S1D) and analyzed the dendritic spine morphology in the cortical pyramidal neurons in P17 mice pups. A dramatic reduction was observed in the number of mature mushroom-shaped spines as compared to those in mice embryonically injected with the control shRNA (Figure S1D).

The effect of TAOK2 knockdown on the stability and morphology of dendritic protrusions was rescued by exogenous expression of wild-type human TAOK2, but not by the kinase-dead mutant TAOK2^{K57A} (Figures S1E and S1F), indicating that the kinase activity of TAOK2 is essential for the stability and morphology of dendritic spines. Together, these data suggest that TAOK2 kinase localizes to dendritic spines in hippocampal neurons and is required for spine morphology and stability both in vitro and in vivo.

Synapses Form Directly on the Dendritic Shaft in Neurons Lacking TAOK2

Dendritic spines mature with an enrichment of postsynaptic scaffolding proteins that recruit and stabilize glutamate receptors, as well as cell adhesion proteins, to form functional synapses (MacGillavry and Hoogenraad, 2015). In DIV18 hippocampal neurons expressing RFP-tagged scaffolding protein PSD-95 along with TAOK2 specific shRNA, PSD95 was localized mostly in the dendritic shaft rather than the immature dendritic protrusions, whereas in control neurons, PSD95 was present in mature spine-heads (Figures 2A and 2B). Immunofluorescence analysis of presynaptic and postsynaptic proteins using antibodies against Bassoon and Homer1a, respectively, revealed that, while in control neurons most excitatory synapses resided on dendritic spines, synapses were rarely located on the dendritic protrusions in neurons with TAOK2 knockdown. Instead, synapses formed directly on the dendritic shaft (Figures 2C–2E). Additionally, accumulation of both NMDA receptors and AMPA receptors to the dendritic protrusions was compromised in TAOK2 knockdown neurons. NR2A/NR2B subunits of NMDA receptors were localized in dendritic shafts rather than spines (Figures S2A and S2B). To visualize AMPA receptors on the cell surface, we transfected neurons with pH-sensitive GFP-tagged GluR1 (SEP-GluR1) (Kopec et al., 2006), along with either control or TAOK2 shRNA. In contrast to the normal enrichment of SEP-GluR1 punctae in mature dendritic spines, more than 80% of the GluR1-SEP punctae were found along the length of the dendritic shaft in TAOK2 depleted neurons (Figures 2F and 2G). Thus, knock down of TAOK2 impairs the enrichment of

(G) Spine density of control and TAOK2 shRNA treated neurons defined as number of protrusions per unit dendritic length (n = 15 per condition, $p < 0.0001$, and t test).

(H) Quantification of the length of protrusion from the base of the dendritic shaft (n = 15 per condition, $p < 0.0001$, and t test with Welch correction). All of the error bars represent SEM.

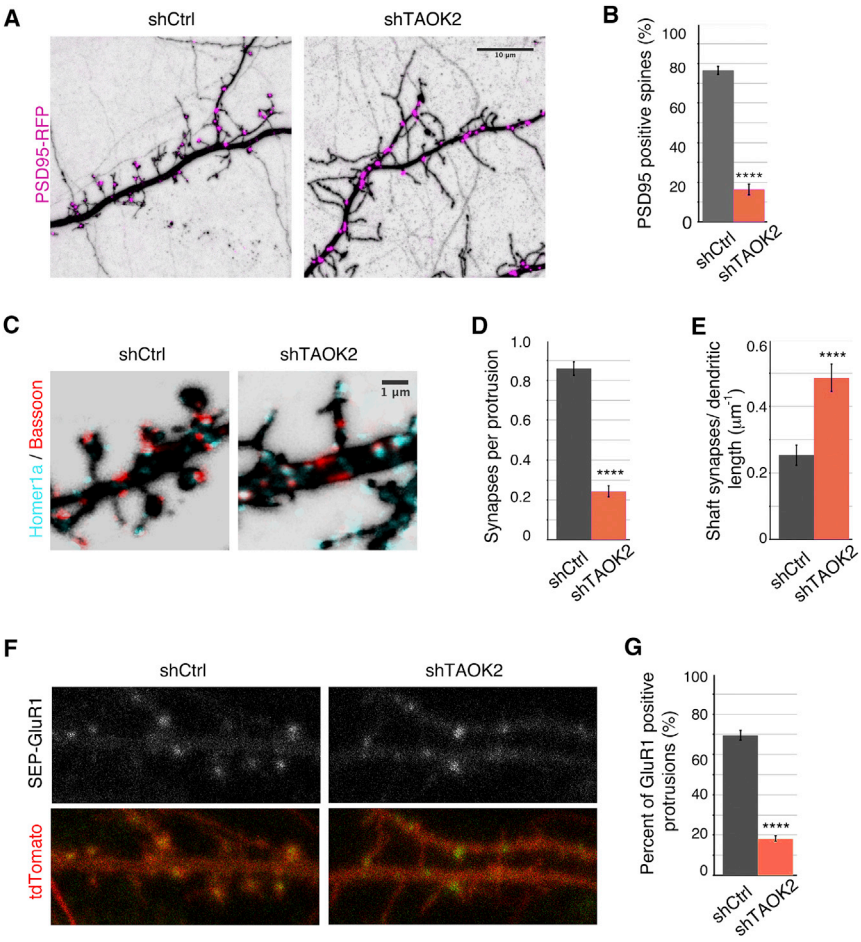

Figure 2. Synapses Are Formed Directly on the Dendritic Shaft in Absence of TAOK2

(A) Hippocampal neurons transfected with either control or TAOK2 shRNA along with RFP-tagged PSD95 to visualize postsynaptic localization of PSD95. The scale bar represents 10 μm.

(B) Percent dendritic protrusions positive for PSD95 ($n = 15$ per condition, $p < 0.0001$, and t test).

(C) DIV18 neurons transfected with either control or shRNA against TAOK2 were fixed and immunostained for presynaptic Bassoon and postsynaptic Homer1a. The co-localization of Bassoon/Homer1a in confocal images was considered as a synapse. The scale bar represents 1 μm.

(D) Number of synapses made on the dendritic protrusions as a fraction of total protrusions ($n = 10$ neurons per condition, $p < 0.0001$, and t test).

(E) Number of synapses made directly on the dendritic shaft per unit dendritic length ($n = 10$ neurons per condition, $p < 0.0001$, and t test). The error bars represent SEM.

(F) Representative confocal images of hippocampal neurons transfected with either control or TAOK2 shRNA (expresses tdTomato under separate promoter) along with pH-sensitive SEP-GluR1. The scale bar represents 5 μm.

(G) Percent of GluR1 positive protrusions ($n = 15$ per condition, $p < 0.0001$, and t test). All of the error bars represent SEM.

the surface localized AMPA receptors into postsynaptic spine compartments.

Compartmentalization of NMDA Receptor-Mediated Ca^{+2} Transients Is Disrupted by TAOK2 Knockdown

To test whether the synapses on the dendritic shaft of neurons with TAOK2 knockdown were functional, we used the lipophilic dye FM4-64 to visualize the presynaptic membrane (Gaffield and Betz, 2006). We found that the presynaptic membrane was apposed directly on the dendritic shaft of TAOK2 knockdown neurons in contrast to the spine localization in control neurons (Figure S3A). Measurement of the amplitude and frequency of miniature excitatory postsynaptic currents (mEPSC) in DIV16-18 hippocampal neurons transfected with control or TAOK2 shRNA revealed comparable amplitude and frequency of the mEPSCs (Figures 3A–3C). In addition, no significant differences were detected in the area, rise time, or decay time of the mEPSCs (Figures S3B–S3D). The ratio of the NMDA mediated slow currents to the AMPA mediated fast currents in hippocampal neurons transfected with TAOK2 shRNA were comparable to the control neurons (Figures S3E–S3G).

Next, we looked into calcium compartmentalization, a major function attributed to the dendritic spines (Adrian et al., 2014; Sabatini et al., 2001; Yuste et al., 2000). Spontaneous NMDA receptor activation can be visualized using calcium sensors when cultured neurons are imaged in absence of Mg^{+2}. Calcium transients generated by NMDA receptors are highly compartmentalized due to the geometrical constraints generated by the spine morphology (Sabatini et al., 2002). In control neurons transfected with the calcium sensor GCaMP6f, reversing the Mg^{+2} block by exposure to artificial cerebrospinal fluid (ACSF) with $0Mg^{+2}$/TTX led to spontaneous calcium spikes that were compartmentalized in the dendritic spines (Figures 3D, top row and 3E; Movie S2). In contrast, in TAOK2 knockdown neurons, most calcium transients were generated directly in the dendritic shaft with almost none in the immature dendritic filopodia (Figures 3D, bottom row and 3E; Movie S3). This observation is consistent with our finding that NMDA receptors were localized in dendritic shafts of neurons lacking TAOK2. In addition, the calcium signals in the TAOK2 knockdown neurons spread out across large areas of the dendritic shaft ranging from submicron to more than 8 μm in length (Figure 3F; Movies S2 and S3). These data suggest that upon TAOK2 depletion, there is a dramatic loss in postsynaptic biochemical compartmentalization in the absence of spine synapses.

Identification of Direct Substrates of TAOK2 Kinase Using Chemical-Genetics and Mass Spectrometry

To delineate the signaling pathway downstream of TAOK2 kinase activity, we employed chemical-genetics and mass spectrometry and identified direct phosphorylation substrates of TAOK2 (Hertz et al., 2010; Ultanir et al., 2012). Briefly, the

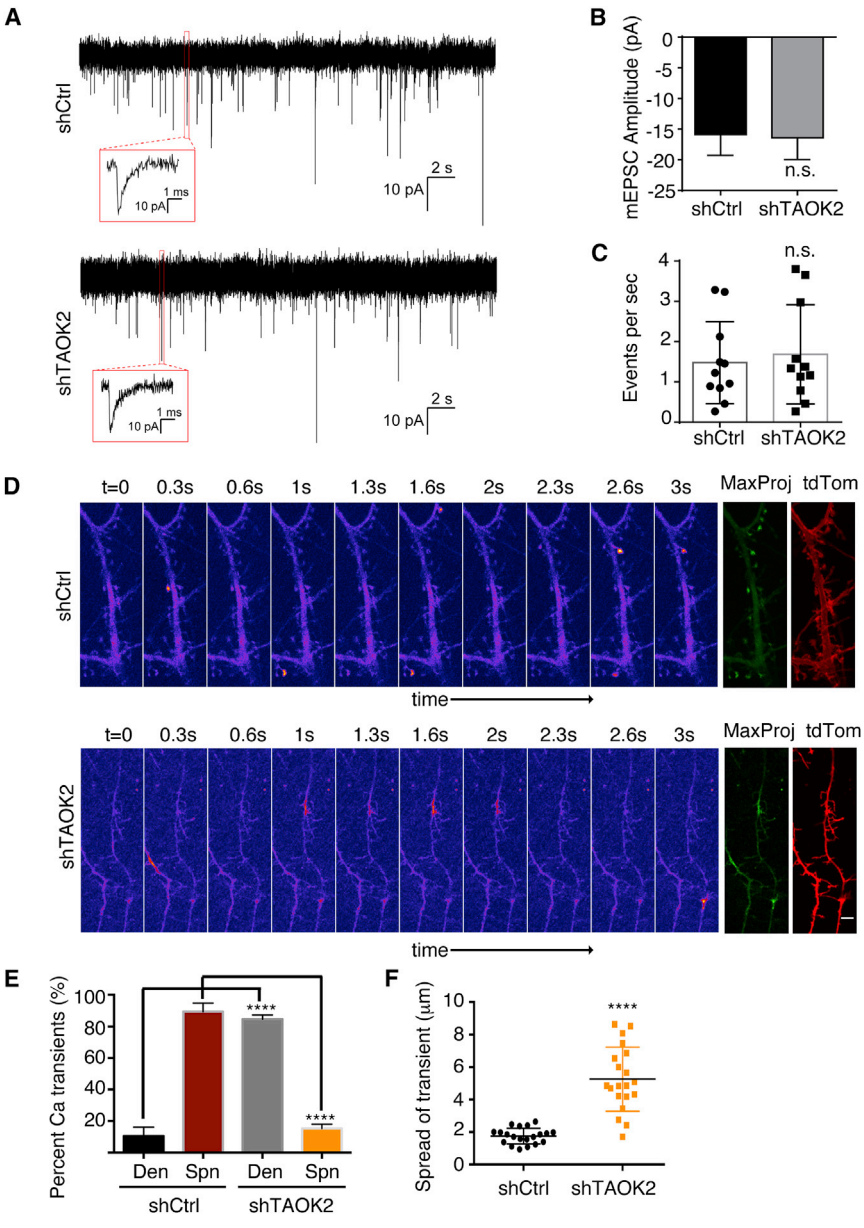

Figure 3. Loss of Dendritic Spines Leads to Defect in Calcium Compartmentalization

(A) Representative traces of miniature excitatory postsynaptic currents measured from DIV16–18 neurons transfected with either control or TAOK2 shRNA. The inset depicts a typical event in higher magnification.

(B) Amplitude of mEPSCs in control and TAOK2 shRNA treated neurons.

(C) Frequency of excitatory events in control and TAOK2 shRNA treated neurons (n = 11–15 neurons from three independent experiments per condition, $p > 0.05$, and t test). The error bars represent SD.

(D) Montages depict sequential frames acquired every 300 ms in time-lapse imaging of DIV16–18 neurons transfected with GCaMP6f along with either control or TAOK2 shRNA. The calcium transients are denoted by higher fluorescence intensity values in the pseudo-color scaled images. A maximum projection image (MaxProj) of all the time frame reveals all the calcium spike events in green. The tdTomato channel is used as a reference for dendritic spine morphology. The scale bar represents 2 µm.

(E) The percent of total calcium transients observed in spine or the dendritic shaft. Three movies per condition were acquired as independent experiments and each spike during the movie was counted (****$p < 0.0001$ and one-way ANOVA with multiple comparisons).

(F) Mean of the distance traversed by the calcium spike during distinct events (n = 20–25 per condition, $p < 0.0001$, and t test with Welch correction). The error bars represent SEM.

method involves substituting the gatekeeper residue in the kinase domain with a smaller amino acid, such that the kinase may utilize a bulkier artificial analog of ATPγS, thereby tagging its direct substrates with a thiophosphate group. The thiophosphorylated substrates are covalently captured by an iodoacetyl resin, specifically eluted by hydrolysis, analyzed by mass spectrometry, and, finally, such phosphopeptides are identified through the ProteinProspector software (Clauser et al., 1999; Guan et al., 2011) (Figure 4C). The gatekeeper residue in the kinase domain of TAOK2, M105, was replaced by a smaller amino acid Ala or Gly (M105A or M105G) to enlarge the ATP binding pocket. The resulting decrease in the kinase activity of TAOK2 was rescued by secondary mutations R97Y and G168A in the kinase domain (Figure 4A). Using autophosphorylation of TAOK2 as a readout of kinase activity in in vitro kinase assays, we found that the engineered analog-sensitive TAOK2 (TAOK2^{AS}) kinase utilized the bulkier ATPγS analogs much more efficiently as compared to unmodified ATPγS. Further, on incubation with mouse brain lysate, numerous proteins were phosphorylated by the TAOK2^{AS}, but not by the kinase-dead TAOK2 (TAOK2^{K57A}) mutant (Figure 4B). To identify downstream direct substrates of TAOK2 that are enriched in the brain, we incubated postnatal mouse brain extracts (P13–P15) with bacterially purified TAOK2^{AS} kinase in the presence of N6-Benzyl-ATPγS, which would bestow putative substrates in the brain lysate with a thiophosphate tag. The thiophosphate-tagged peptides along with cysteine-containing peptides were bound to iodoacetyl agarose beads. A hydrolysis reaction ensured that only the thiophosphate containing peptides were specifically eluted (Figure 4C). Eluted peptides were identified by mass spectrometry (Figure 4D) and analyzed by the ProteinProspector software (Guan et al., 2011). Substrates identified by mass spectrometry in the analog-sensitive TAOK2^{AS}, but not in the kinase-dead TAOK2^{K57A}, reaction were shortlisted. Several proteins known to be involved in dendritic spine formation, cytoskeletal remodeling, ciliogenesis, and axonal growth were identified (Figure 4E).

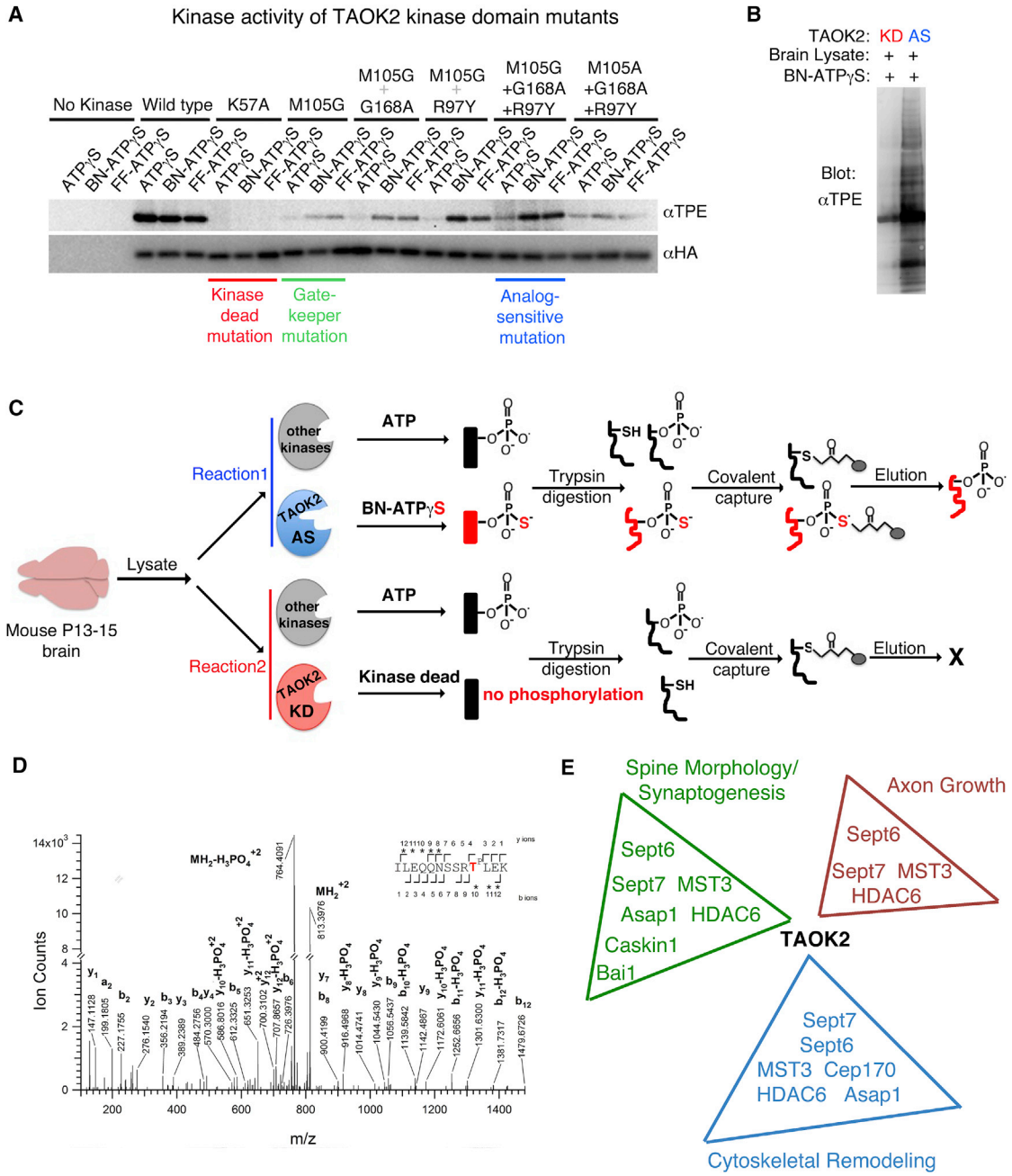

Figure 4. Mass Spectrometry Based Identification of TAOK2 Substrates in the Brain

(A) Kinase activity of the engineered TAOK2 mutants was measured to screen for the analog sensitive mutation using the autophosphorylation of TAOK2 as a readout. HA-tagged TAOK2 kinase domain (1–320 amino acids) harboring the depicted mutations was incubated with either ATPγS or the analogs N6-Benzyl-ATPγS (BN) and N6-Furfuryl-ATPγS(FF) in an in vitro kinase reaction followed by alkylation using p-nitrobenzyl mesylate (PNBM) to produce thiophosphate-ester. Western blot of the phosphorylated TAOK2 mutants was probed with HA antibody and thiophosphate-ester specific antibody to visualize the total amount of TAOK2 mutant and the kinase activity of the mutant, respectively. The kinase dead (K57A), gatekeeper mutation (M105G), and the analog-sensitive mutation (M105G+G168A+R97Y) are highlighted.

(B) Brain lysate from P13 mouse was incubated with either the kinase-dead (KD) or the analog-sensitive (AS) TAOK2 and probed for total amount of phosphorylated proteins using the thiophosphate-ester specific antibody.

(C) Schematic depicts the workflow for TAOK2 substrate labeling and subsequent covalent capture prior to identification through mass spectrometry.

(D) Representative spectrum obtained from the mass spectrometry analysis of phosphorylated peptides enriched in the analog sensitive condition, but not in the kinase dead reaction. This spectrum was obtained by HCD fragmentation from a precursor ion with m/z value 813.3971^{+3}, corresponding to a phosphorylated

(legend continued on next page)

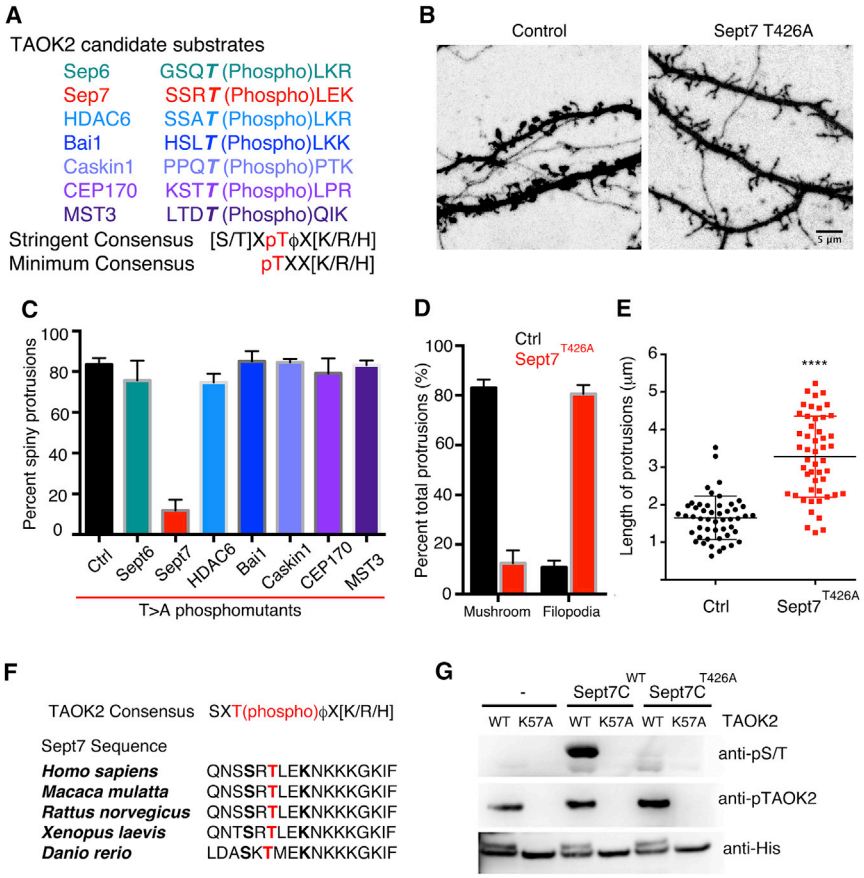

Figure 5. Phosphorylation of Sept7 by TAOK2 Is Required for Dendritic Spine Formation

(A) Identified candidate substrates of TAOK2 from the mouse brain, with the threonine phosphorylation sites (bold) identified by mass spectrometry and the consensus sequence for phosphorylation by TAOK2.

(B) Representative images of dendritic spines of DIV18 hippocampal neurons transfected with GFP alone and GFP along with the Septin7 phosphomutant (T426A). The scale bar represents 5 μm.

(C) Percent of mature mushroom shaped spine protrusions in control neurons and in neurons transfected with the identified phosphomutants (n = 10–12 from three independent experiments, ****p = 0.0001, n.s. = p > 0.05, and one-way ANOVA).

(D) Classification of the dendritic protrusions in control and Sept7^{T426A} expressing neurons on the basis of mature mushroom spines or long filopodia as a percent of total dendritic protrusions. Three experiments with ten neurons per group were analyzed using multiple t tests to compare the two groups in each category.

(E) Average length of individual dendritic protrusions in control and Sept7 phosphomutant expressing neurons where each dot represents individual data points. The lengths from three independent experiments were pooled and analyzed (n = 50 protrusions per condition, ****p < 0.0001, and unpaired t test with Welch correction). All of the error bars represent SEM.

(F) Multiple sequence alignment of the C-terminal tail of Sept7 shows highly conserved sequence and conserved site of phosphorylation from fish to human. The site of phosphorylation is shown in red.

(G) Purified TAOK2 wild-type (WT) or kinase dead (K57A) was incubated either alone, with GST-tagged wild-type, or phosphomutant Sept7 C-terminal tails (Sept7C^{WT} or Sept7C^{T426A}). Phosphorylation of Sept7 C-terminal tail was detected in a western blot by probing with a pan phospho-serine/threonine (pS/T) antibody. The phosphorylated TAOK2 representing the active kinase is detected by antibody against pTAOK2 and total kinase by an antibody against the His-tag.

Many of the candidate substrates conformed to the specific consensus sequence [S/T]-X-**T**^{P}−Φ−X-[R/K/H], where "Φ" is a hydrophobic residue and "X" denotes any residue. The minimum strict consensus that we found was (**T**)^{P}-X-X[R/K/H], where the amino acid at the p+3 position is a basic residue (Figure 5A). The phosphorylation site on those candidate substrates that met the consensus sequence criteria and were found in at least two of four independent mass spectrometry experiments was found to be conserved between mouse and human (Figure S4A). This suggests that the phosphorylation of the identified direct substrates by TAOK2 likely represents physiologically relevant and distinct downstream signaling pathways.

TAOK2 Phosphorylation of Septin7 Is Required for Dendritic Spine Formation

Next, we examined the role of the identified putative direct substrates of TAOK2 in regulating dendritic spine morphogenesis. By mutating the site of phosphorylation determined by mass spectrometry from threonine to alanine, we generated the phosphomutant versions of the identified substrates (Figure S5A). We found that in hippocampal neurons only expression of the septin7 phosphomutant, Sept7^{T426A}, led to a dramatic loss in mature dendritic spines and was accompanied by an increase in the density of immature filopodia (Figures 5B–5D). Expression of Sept7^{T426A} also led to an increase in the density of the dendritic protrusions (Figure S5B), which were filopodia-like, thin, and long protrusions similar to those of neurons expressing kinase-dead TAOK2. Compared to the mean dendritic spine length of 1.5 μm in control neurons, the average length of filopodia in Sept7^{T426A} expressing neurons increased to 3.5 μm (Figure 5E). While we cannot exclude the contribution of other identified substrates in dendritic spine morphogenesis, our data indicate that Sept7 phosphorylation by TAOK2 is required for dendritic spine formation and maturation.

tryptic peptide spanning residues I417 to K429 of mouse septin7, phosphorylated on T426 (phosphorylated threonine is shown in the sequence as **T**^{P}). The observed b and y product ion peaks are labeled accordingly with the subscripts denoting their position in the identified peptide.

(E) Gene Ontology analysis of proteins identified as direct substrates of TAOK2 reveals enrichment in processes such as dendritic spine formation/synaptogenesis, axon growth, cytoskeletal remodeling, and ciliogenesis.

Septin7 C-Terminal Tail Is Directly Phosphorylated by TAOK2 at Residue T426

First identified in yeast, septins form an essential component of the cellular cytoskeleton along with actin, microtubules, and intermediate filaments (Mostowy and Cossart, 2012). The structure of septins is highly conserved with an N-terminal GTP-binding domain, followed by a coiled-coil region, and an unstructured C-terminal tail. The C-terminal tail has been implicated in mediating protein-protein interactions, as well as lateral interactions between septin oligomers (de Almeida Marques et al., 2012; Finnigan et al., 2015). Our mass spectrometry data revealed the site of phosphorylation on Sept7 to be T426 in the C-terminal tail of the protein, within a sequence conserved from fish to human (Figure 5F). Using an in vitro kinase assay with purified TAOK2 kinase-domain (1–320 amino acids) and Sept7 C-terminal tail (321–438 amino acids), we found that TAOK2^{WT} phosphorylated purified GST-tagged Sept7-C^{WT}, but not Sept7-C^{T426A}. The kinase-dead TAOK2^{K57A} failed to phosphorylate either, indicating that T426 is the only residue in the C-terminal tail of Sept7 that is directly phosphorylated by TAOK2 (Figure 5G). As the full-length septin7 precipitates out of solution during purification unless expressed as a heteromer with septin6 (Kremer et al., 2005), we purified the full-length His-Sept6/Sept7 complex from bacteria. We confirmed that the full-length Sept6/7 complex is also phosphorylated by purified TAOK2 kinase in vitro, but not by the kinase-dead TAOK2^{K57A} (Figure S6A). We further generated a phospho-specific antibody against the Sept7 C-terminal peptide with phosphorylated T426 (p-T426) and showed that this phosphospecific antibody detected GST-Sept7-C^{WT} phosphorylated by TAOK2, but not Sept7-C^{T426A} or other phosphorylated proteins (Figure S6B). Incubation of Sept7-C^{WT} with purified TAOK2 for increasing lengths of time resulted in progressively greater TAOK2 phosphorylation of Sept7 at T426 as a function of time (Figures S6C and S6D). Next, we tested whether TAOK2 phosphorylates endogenous Sept7 in vivo using the generated pT426 antibody. Knock down of TAOK2 in hippocampal neurons significantly decreased the levels of endogenous phosphorylated Sept7 as compared to control neurons (Figures 6A and 6B). Moreover, incubation of mouse brain lysate with purified TAOK2 in a kinase assay led to phosphorylation of endogenous Sept7 at T426 (Figure S6E). To test whether phosphorylated Sept7 is sufficient to rescue the loss of dendritic spines on TAOK2 knockdown, we expressed the phosphomimetic Sept7, Sept7^{T426D}, in neurons transfected with shRNA against TAOK2. Phosphomimetic Sept7^{T426D} greatly rescued the loss of dendritic spines, while expression of Sept7^{WT} or Sept7^{T426A} did not, thereby placing Sept7 phosphorylation downstream of TAOK2 in facilitating the maturation of dendritic spines (Figures 6C and 6D). Expression of the phosphomimetic Sept7^{T426D} in control neurons led to a slight increase in the number of mature mushroom spines when compared to expression of Sept7^{WT}, indicating that the phosphomimetic Sept7 has a stabilizing effect on dendritic spine structure (Figures 6C and 6D). To determine the effect of the Sept7 phosphorylation on the dynamics of the dendritic protrusions, we performed time-lapse imaging of neurons transfected with either Sept7^{T426A} or Sept7^{T426D} along with tdTomato. While dendritic spines in Sept7^{T426D} expressing neurons were stable and enriched with Sept7, the protrusions in neurons expressing Sept7^{T426A} were highly dynamic and motile (Movie S4). These data provide further evidence that Sept7 is phosphorylated by TAOK2 at T426 both in vitro and in vivo and is required for dendritic spine maturation.

We next investigated whether Sept7 phosphorylation by TAOK2 was required for spine-synapse formation and compartmentalization of NMDA receptor-mediated calcium influx. We found that in hippocampal neurons expressing the phosphomutant Sept7^{T426A}, 77% of synapses as determined by co-localization of postsynaptic and presynaptic protein PSD95 and bassoon were formed directly on the dendritic shaft (Figures 6E and 6F). Moreover, in neurons co-transfected with the calcium indicator RGeco1.2 along with either GFP-tagged Sept7^{T426A} or Sept7^{T426D}, high speed time-lapse imaging in Mg^{+2} free ACSF solution revealed an average of 82% of calcium transients in the dendritic shaft of neurons expressing Sept7^{T426A} as opposed to a mean 86% of compartmentalized calcium transients in the dendritic spines of Sept7^{T426D} expressing neurons (Figures 6G and 6H).

Sept7 Localizes to Dendritic Spines on Phosphorylation by TAOK2

Expression of phosphomimetic or phosphomutant Sept7 in HEK293 cells did not perturb the filament forming ability of Sept7 (Figure S7A). On transfection of neurons with GFP-tagged Sept7^{T426A} or Sept7^{T426D}, we found that both localized at the base of the dendritic protrusions and along the dendritic shaft of the neuron (Figures 6C and 7A). However, we found that Sept7^{T426D} expression led to an increased localization of Sept7 to the dendritic spine head as compared to neurons transfected with Sept7^{T426A} (Figures 6C and 7A; Movie S4).

We next tested whether phosphorylation of Sept7 at T426 changed its dynamics of assembly. By measuring the fluorescence recovery after photobleaching, we found that GFP-tagged Sept7 ^{T426D} enriched at the spines was more stable than the phosphomutant Sept7 ^{T426A} that accumulated at the base of the dendritic spine. While about 75% of the photobleached Sept7^{T426A} recovered in a period of 20 min, only 50% of the phosphomimetic Sept7^{T426D} recovered, indicating that phosphorylation of Sept7 affects its mobility (Figures 7B and 7C). These data provide evidence that direct phosphorylation of Sept7 by TAOK2 promotes Sept7 localization to the dendritic spine head as well as reduces the mobility of Sept7 in the spine. We hypothesize that this stable pool of phosphorylated Sept7 is required for dendritic spine maturation.

Next, we investigated which upstream signals might activate the TAOK2-Sept7 pathway to induce dendritic spine maturation. A previous study has shown that TAOK2 is activated through phosphorylation at residue S181 by the secreted semaphorin Sema3a signaling through its receptor Neuropilin1 (de Anda et al., 2012). In addition, the hippo kinase mammalian homolog MST3 directly phosphorylates TAOK2, but at a different residue T441 (Ultanir et al., 2014). To test if Sema3a could regulate Sept7 phosphorylation, we added purified recombinant Sema3a to cultured neurons for 4 hr and found that the level of phosphorylated Sept7 was unchanged both by western blot and immunofluorescence assessments, indicating that Sema3a was unlikely to influence the TAOK2-Sept7 pathway (Figures S7B and S7C). Next, we tested

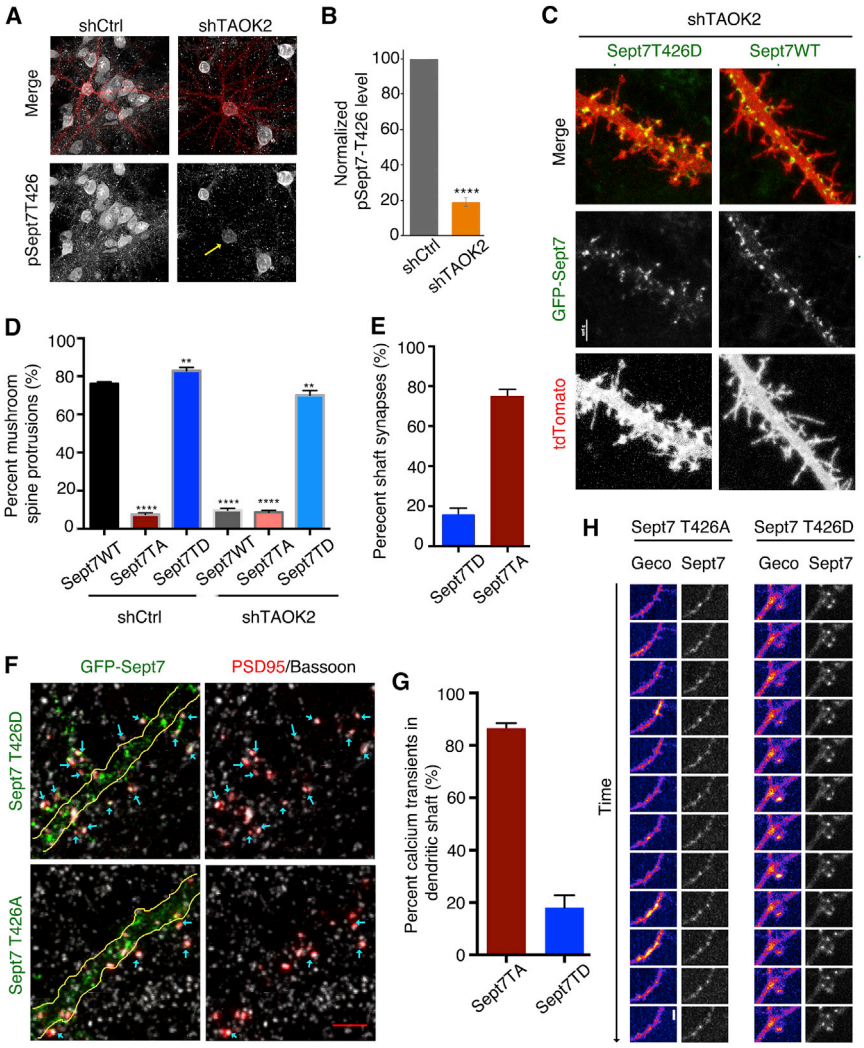

Figure 6. Sept7 Is Directly Phosphorylated by TAOK2 at Its C-terminal Tail and Is Required for Synapse Location and Calcium Compartmentalization

(A) Hippocampal neurons transfected with control or shRNA against TAOK2 were immunostained using an antibody against phosphorylated Sept7 (pT426) to detect the endogenous levels of phosphorylated Sept7. The transfected cells are detected by tdTomato expression.

(B) Mean pSept7 fluorescence intensity in TAOK2 knockdown neuronal soma normalized to the mean of the fluorescence in the control treated soma ($n = 10$ neurons per condition, $p < 0.0001$, and t test).

(C) Hippocampal neurons at DIV15 were transfected with TAOK2 shRNA (tdTomato) along with co-expression of GFP-tagged Sept7-WT or Sept7-T426D. The scale bar represents 3 μm.

(D) Percent of dendritic protrusions that were mushroom spines upon co-expression of GFP-tagged Sept7-WT, Sept7-T426A, or Sept7-T426D with either control or TAOK2 shRNA ($n = 15$ per experimental condition, **** = $p < 0.0001$, ** = $0.01 > p > 0.001$, and * = $0.05 > p > 0.01$ one-way ANOVA with Holm-Sidak's multiple comparison test). The significance values are shown in respect to the first column.

(E) Synaptic localization in neurons expressing GFP-tagged Sept7 T426A or Sept7 T426D along with RFP-PSD95 was determined by immunofluorescence assay with antibodies against GFP and presynaptic protein Bassoon.

(F) The synaptic localization was quantified as a percent of total synaptic punctae that were present along the dendritic shaft. The error bars represent SEM.

(G) DIV14 hippocampal neurons were transfected with GFP-tagged Sept7 T426A or Sept7 T426D along with the genetically encoded red calcium indicator RGeco1.2 and imaged at DIV16 in Mg+2 free media to visualize calcium transients.

(H) The calcium transients were quantified as the percent of total calcium transients observed in the shaft or protrusions in neurons expressing Sept7T426A or Sept7T426D. The error bars represent SEM.

if MST3 was required for Sept7 phosphorylation by knocking down MST3 and probing for phosphorylated Sept7. Indeed, neurons transfected with MST3 shRNA or TAOK2 shRNA showed lower levels of pSept7 as revealed by western analysis (Figure 7D) and immunofluorescence (Figures 7E and 7F). Moreover, MST3 mediated phosphorylation induced TAOK2 to localize in dendritic spines as revealed by the pT441 antibody, whereas TAOK2 phosphorylated by Sema3a as determined by the pS181 antibody was mostly localized to the soma and dendrites consistent with its role in dendritic growth, but not dendritic spine maturation (Figure S7D). These data together provide evidence for a role of the MST3-TAOK2-Sept7 pathway in the maturation of dendritic spines.

Phosphorylated Sept7 Interacts and Stabilizes PSD95 in the Dendritic Spine

In neurons transfected with phosphomimetic or wild-type Sept7 along with the synaptic scaffolding protein PSD95, we observed much greater co-localization of Sept7^{T426D} with PSD95 in the spine head as compared to Sept7^{WT} (Figures 7G and 7H). This prompted us to test whether PSD95 associates with the C-terminal tail of Sept7 and, if so, whether this interaction is dependent upon phosphorylation by TAOK2. Using the pSept7 (T426) antibody, we found that phosphorylated Sept7 co-immunoprecipitated with PSD95 from mouse brain lysates, indicating that phosphorylated Sept7 and PSD95 interact in vivo (Figure S7E). To test whether phosphorylation of the Sept7 C-terminal tail was required for the interaction, we incubated purified GST-tagged wild-type and phosphomutant Sept7 C-terminal tails with either wild-type or kinase-dead TAOK2 in a kinase buffer to allow phosphorylation. The phosphorylated proteins were then incubated with brain lysate followed by addition of glutathione beads to pull down the GST-tagged proteins. The precipitated protein fraction was probed with antibodies against PSD95 in a western blot to test for interaction with PSD95. We found that TAOK2^{WT}, but

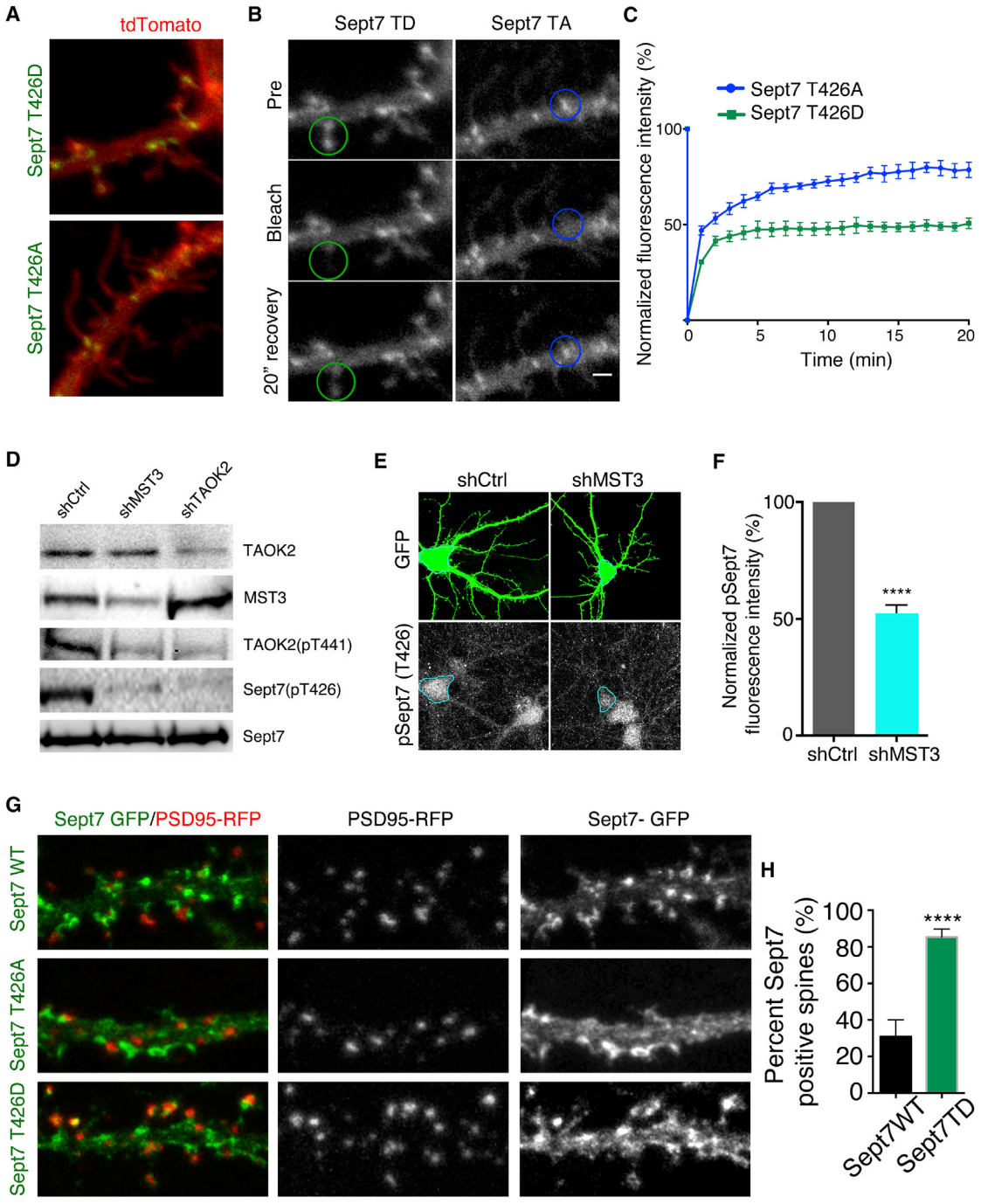

Figure 7. Sept7 Localization and Mobility Is Regulated by TAOK2 Mediated Phosphorylation

(A) Representative images of hippocampal neurons transfected with TdTomato along with GFP-tagged Sept7^{T426A} or Sept7^{T426D} show an increase in Sept7 localization in spines on expression of the phosphomimetic T426D mutant. The scale bar represents 3 μm.

(B) Montage of images from hippocampal neurons expressing GFP-tagged Sept7^{T426A} or Sept7^{T426D} depict prebleach image, photobleached image, and fluorescence recovery at 20 min after bleaching of the Sept7 fluorescence in the region of interest (ROI) marked by the circle.

(C) Graph depicts the mean normalized fluorescence intensity in ROI of neurons expressing either GFP-tagged Sept7^{T426A} (blue) or Sept7^{T426D} (green) over 20 min where fluorescence intensity was measured every min. The error bars are SEM and n = 6 per condition. The scale bar represents 3 μm.

(D) Western blot of neuronal lysates obtained from cultured hippocampal neurons transduced with virus expressing control shRNA or shRNA against MST3 and TAOK2 depicts the changes in levels of phosphorylated Sept7 (T426) and phosphorylated TAOK2 (T441) on knock down of either TAOK2 or MST3.

(E) Hippocampal neurons were transfected at DIV9 with control or MST3 shRNA and the levels of phosphorylated Sept7 were visualized at DIV12 by immunofluorescence assay using the pSept7 T426 antibody.

(legend continued on next page)

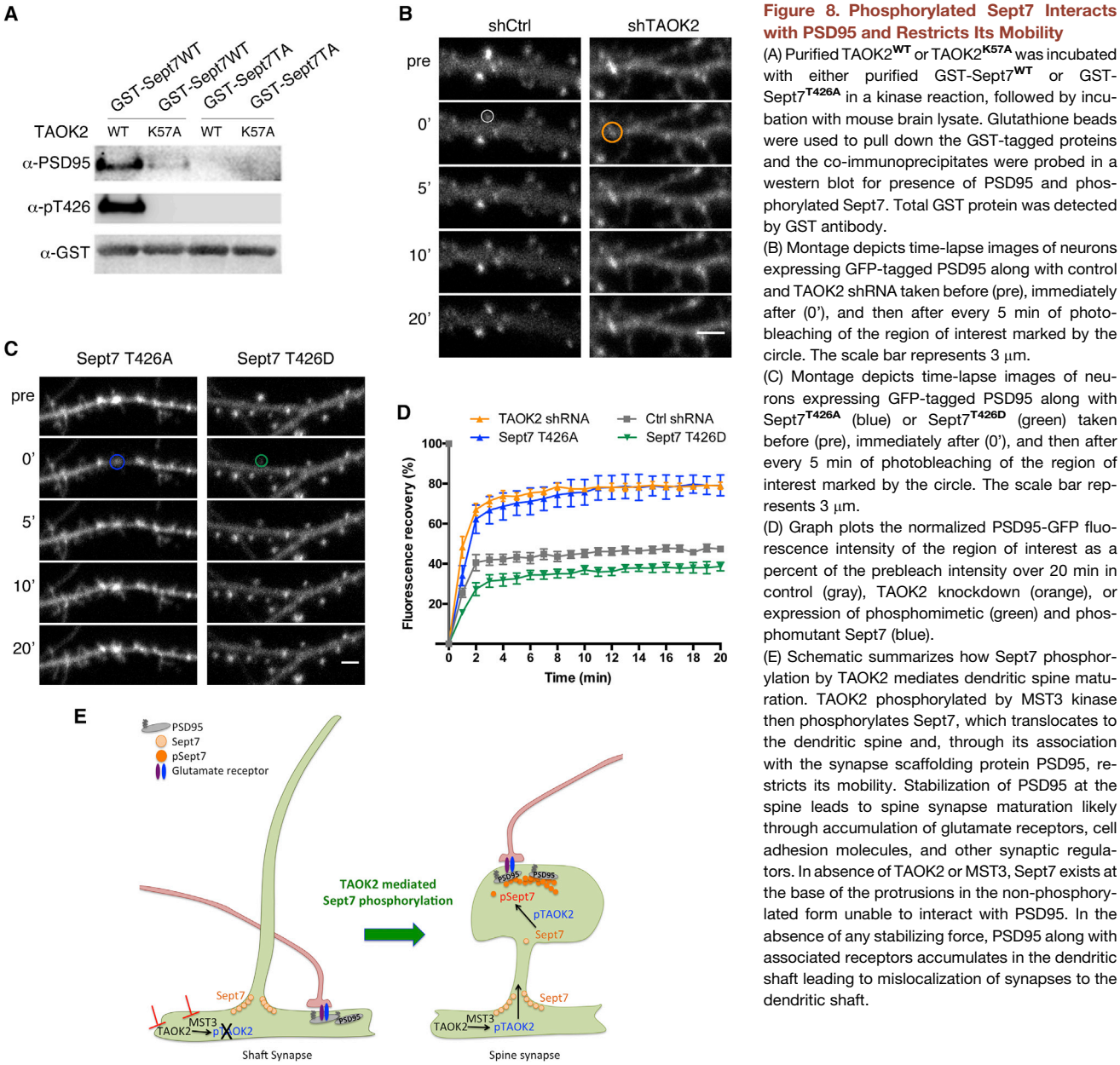

Figure 8. Phosphorylated Sept7 Interacts with PSD95 and Restricts Its Mobility

(A) Purified TAOK2^{WT} or TAOK2^{K57A} was incubated with either purified GST-Sept7^{WT} or GST-Sept7^{T426A} in a kinase reaction, followed by incubation with mouse brain lysate. Glutathione beads were used to pull down the GST-tagged proteins and the co-immunoprecipitates were probed in a western blot for presence of PSD95 and phosphorylated Sept7. Total GST protein was detected by GST antibody.

(B) Montage depicts time-lapse images of neurons expressing GFP-tagged PSD95 along with control and TAOK2 shRNA taken before (pre), immediately after (0'), and then after every 5 min of photobleaching of the region of interest marked by the circle. The scale bar represents 3 μm.

(C) Montage depicts time-lapse images of neurons expressing GFP-tagged PSD95 along with Sept7^{T426A} (blue) or Sept7^{T426D} (green) taken before (pre), immediately after (0'), and then after every 5 min of photobleaching of the region of interest marked by the circle. The scale bar represents 3 μm.

(D) Graph plots the normalized PSD95-GFP fluorescence intensity of the region of interest as a percent of the prebleach intensity over 20 min in control (gray), TAOK2 knockdown (orange), or expression of phosphomimetic (green) and phosphomutant Sept7 (blue).

(E) Schematic summarizes how Sept7 phosphorylation by TAOK2 mediates dendritic spine maturation. TAOK2 phosphorylated by MST3 kinase then phosphorylates Sept7, which translocates to the dendritic spine and, through its association with the synapse scaffolding protein PSD95, restricts its mobility. Stabilization of PSD95 at the spine leads to spine synapse maturation likely through accumulation of glutamate receptors, cell adhesion molecules, and other synaptic regulators. In absence of TAOK2 or MST3, Sept7 exists at the base of the protrusions in the non-phosphorylated form unable to interact with PSD95. In the absence of any stabilizing force, PSD95 along with associated receptors accumulates in the dendritic shaft leading to mislocalization of synapses to the dendritic shaft.

not the kinase-dead TAOK2^{K57A}, phosphorylated Sept7-C^{WT}, and neither phosphorylated Sept7-C^{T426A}, as expected. Moreover, endogenous PSD95 from the brain lysate was pulled down by Sept7-C^{WT} that was incubated with wild-type TAOK2, but not the kinase-dead mutant, whereas mutation of T426 to alanine completely abolished the interaction between Sept7 C-terminal tail and PSD95 (Figures 8A, S7F, and S7G). In addition, when incubated with the kinase-dead TAOK2^{K57A}, neither the wild-type nor the phosphomutant Sept7 could pull down PSD95 from the brain lysate, indicating that Sept7 associates with PSD95 via its C-terminal tail in a strictly phosphorylation-dependent manner (Figure 8A). Given that 10%–15% of endogenous Sept7 was pulled down with PSD95 from mouse brain lysates, it appears that a small fraction of Sept7 is phosphorylated by TAOK2 in vivo.

Stabilization of the postsynaptic machinery including the scaffolding machinery and glutamate receptors can dramatically

(F) Phosphorylation level of Sept7 was quantified as a percent of the total normalized fluorescence intensity. The error bars are SEM and n > 7 per condition.

(G) Higher magnification images comparing localization of GFP-tagged Sept7^{WT} and Sept7^{T426D} along with RFP-tagged PSD95 (red). The merged image highlights co-localization between Sept7^{T426D} and PSD95. The scale bar represents 2 μm.

(H) Percent dendritic spines positive for Sept7 in neurons transfected with either Sept7^{WT} or Sept7^{T426D} mutant (n = 15–20 neurons per condition, $p < 0.0001$, and t test). The error bars are SEM.

affect spine stability (Hering and Sheng, 2001). PSD95 among the various MAGUK proteins is very precisely targeted to the synapse, and this synapse localization requires N-terminal palmitoylation, PDZ domains, as well as its C-terminal domain for protein-protein interactions (Kim and Sheng, 2004; Sturgill et al., 2009). To test whether the stable spine-associated population of Sept7 could associate with PSD95 and restrict its mobility, thereby mediating spine stability and its maturation, we measured the effect of TAOK2 mediated Sept7 phosphorylation on the mobility of PSD95 in dissociated neurons. Neurons were transfected with GFP-tagged PSD95 along with either control shRNA, TAOK2 specific shRNA, phosphomutant Sept7^{T426A}, or phosphomimetic Sept7^{T426D}. Individual PSD95-GFP punctae in each condition were then photobleached, and the extent of fluorescence recovery was measured over a period of 20 min (Figures 8B–8D). The mobile fraction of PSD95 increased from 45.75% in control to 77.76% in TAOK2 knockdown neurons. Likewise, approximately 77% of PSD95 was in the mobile fraction in neurons expressing the phosphomutant Sept7^{T426A}. In contrast, expression of the phosphomimetic Sept7^{T426D} further reduced the mobile fraction of PSD95 to 36.5% of the total population, as compared to the 45% in control neurons (Figure 8D). These data indicate that the mobility of PSD95 is regulated by TAOK2 mediated phosphorylation of Sept7, providing a direct mechanism for dendritic spine stability. Collectively, our study suggests that phosphorylation by TAOK2 on the C-terminal tail of Sept7 acts as a switch for the dendritic spine localization of Sept7, for its interaction with postsynaptic scaffold protein PSD95, as well as for the mobility of PSD95 (Figure 8E).

DISCUSSION

TAOK2 Regulates Dendritic Spine Maturation and Calcium Compartmentalization

Recently, we identified TAOK2 as one of the direct substrates of MST3 kinase, a member of the hippo kinase family required for dendritic spine formation. MST3 mediated phosphorylation of TAOK2 is required for its interaction with Myosin Va and for dendritic spine formation (Ultanir et al., 2014).

In this study, we show that TAOK2 localizes to the dendritic spines in hippocampal neurons, and that it is important for dendritic spine formation both in vitro and in vivo. TAOK2 is required for the stability of dendritic protrusions, and in its absence synapses form directly on the dendritic shaft. Electrophysiological measurements of baseline mEPSCs and AMPA/NMDA ratios revealed no detectable difference between control and TAOK2 knockdown neurons, indicating that functional synapses can form directly on the dendritic shaft in the absence of stable spine compartments. Although synapses were functional, we found that synapses on the dendritic shaft were defective in compartmentalizing postsynaptic calcium. Our study shows that decoupling the synapse from the confines of the dendritic spine leads to loss of compartmentalization of biochemical signaling, reinforcing the notion that different spine morphologies might represent distinct states of compartmentalization (Lee et al., 2012). This has significant implications in spine plasticity both during development and in learning and memory.

Identification of Direct TAOK2 Substrates and Phosphorylation Sites

To uncover direct neuronal targets of TAOK2, we employed a chemical-genetic strategy wherein substrates were specifically labeled by an engineered kinase followed by mass spectrometry-based identification. Our results reveal that TAOK2 phosphorylation follows the consensus sequence [S/T]-X-**T^{P}**$-\Phi-$X-[R/K/H]. Among the identified substrates of TAOK2 are several proteins affecting axonal growth, ciliogenesis, dendritic spine morphology, and regulators of actin and microtubule cytoskeleton. TAOK2 is a known regulator of actin and microtubule dynamics (King and Heberlein, 2011; Moore et al., 2000), dendritic spine morphology (Ultanir et al., 2014; Yasuda et al., 2007), and axonal growth (de Anda et al., 2012; Kapfhamer et al., 2013). Recently, reports of ciliary dysfunction in 16p11.2 copy number variations have emerged (Migliavacca et al., 2015). Whether and how TAOK2 is involved in ciliogenesis is of interest in light of our finding that several of TAOK2 substrates are proteins enriched in the cilia.

Mutational analysis of identified candidates in our study revealed that TAOK2 mediated phosphorylation of the cytoskeletal GTPase Sept7 is required for dendritic spine maturation. However, we cannot exclude contributing roles of the other TAOK2 candidate substrates in the process, as not all phosphomutants are dominant negative in function. Among the identified proteins, Bai1, a G protein coupled receptor (GPCR) adhesion protein is a known regulator of synaptogenesis (Duman et al., 2013) and is involved in synaptic plasticity and learning (Zhu et al., 2015). Sept6 functions in both dendrite spine formation and axonal growth (Cho et al., 2011; Hu et al., 2012). We did not include Asap1, an ArfGAP in our phosphomutant analysis, as the site of phosphorylation is not conserved in humans (Figure S4A). It is important to note, however, that Asap1 has been implicated in dendritic spine formation in dentate gyrus neurons (Jain et al., 2012), along with a role in ciliogenesis. HDAC6 is a microtubule deacetylase involved in axon outgrowth and ciliogenesis; interestingly, it also interacts with Sept7 (Ageta-Ishihara et al., 2013). Further analysis of these identified candidates could provide mechanistic insight regarding the role of TAOK2 in diverse cellular processes.

Septin Cytoskeleton as a Regulator of Dendritic Spine Structure

By creating diffusion barriers and acting as scaffolds to recruit signaling molecules, septins contribute to the organization of diverse intracellular structures such as the budding neck of yeast, base of the cilium, annulus of the spermatozoa, and the base of the dendritic spines in neurons (Beites et al., 1999; Caudron and Barral, 2009; Ewers et al., 2014; Mostowy and Cossart, 2012; Sirajuddin et al., 2007; Weirich et al., 2008). The C-terminal tail of septins is thought to mediate lateral interactions between septin oligomers, promote stability of the filament, and recruit other interacting proteins to the septin scaffold (de Almeida Marques et al., 2012; Finnigan et al., 2015). Knock down of Sept7 leads to increased immature protrusions and decreased complexity of the dendritic arbor in hippocampal neurons (Tada et al., 2007; Xie et al., 2007). Interestingly, electron microscopy has revealed the presence of Sept7 complex primarily at the base of the spine, dendrites, and axon, but also in the spine

heads (Ewers et al., 2014). Localized at the base of the dendritic spine, Sept7 reduces the rate of diffusion of membrane bound, but not cytosolic, proteins in and out of the spine (Ewers et al., 2014). The role of septins in synaptic structure and plasticity has not been reported so far, and, in particular, the role of post-translational modification of septins to regulate their function was hitherto unknown.

Our study shows that the C-terminal tail of Sept7 is directly phosphorylated by TAOK2, and that this phosphorylation at residue T426 is important for dendritic spine structure, synapse localization, and compartmentalization of NMDA receptor-mediated calcium influx. Phosphorylation of Sept7 did not lead to any observable change in septin oligomerization, however, our study indicates that phosphorylation at T426 promotes Sept7 localization to the spine head. Our finding is consistent with prior studies showing that Sept7 is enriched in the postsynaptic density fraction of brain lysate (Xie et al., 2007), and that a small fraction of total Sept7 was localized to the spine head as revealed by electron microscopy (Ewers et al., 2014). In addition, our data show that phosphorylated Sept7 co-localizes with PSD95 in the spine head, and that Sept7 interacts with endogenous PSD95 in a phosphorylation-dependent manner. Furthermore, by measuring fluorescence recovery after photobleaching, we observed that phosphorylated Sept7 decreases the mobility of PSD95.

Based on our findings, we propose that early during spine development, Sept7 localizes at the base of dendritic filopodia. As the neuron matures, TAOK2 phosphorylates Sept7, which then localizes to the spine head, where it stabilizes the synapse by binding to and restricting the mobility of PSD95 in the spine. PSD95 stability at the spine leads to compartmentalization of the synaptic machinery including NMDA receptors and AMPA receptors in the dendritic spine. Upon depletion of TAOK2, Sept7 primarily exists in the non-phosphorylated form and is unable to interact with PSD95. In the absence of any stabilizing interaction, PSD95 is localized to the dendritic shaft, where it recruits the postsynaptic machinery to form mislocalized synapses that are defective in calcium compartmentalization (Figure 8E).

TAOK2 Kinase and Septins in Neurological and Psychiatric Diseases

TAOK2 is one of the 29 genes in the 16p11.2 genomic locus associated with neurodevelopmental and psychiatric disorders. The 16p11.2 CNV phenotype is complicated and heterogeneous, with diverse phenotypes reflecting outcome of one or a combination of the 29 genes in the locus. Analysis from human patients shows a positive correlation of several of these, namely TAOK2, MAPK3, MVP, KIF22, ALDOA, and KCTD13 mRNA, with the change in brain anatomical structures in autism (Maillard et al., 2015). Future efforts are required to explore the differential contribution of these genes in the neuropathology of 16p11.2 CNVs.

Dysfunction of septins is associated with synaptic defects and neurodegeneration (Marttinen et al., 2015). Interestingly, in schizophrenia patients, the levels of Sept7 mRNA in the cortical tissue were found to be significantly decreased in comparison to control population (Ide and Lewis, 2010). Abnormal levels of both activated TAOK2 and septins have been detected in the neurofibrillary tangles in Alzheimer's disease patients (Tavares et al., 2013). Whether phosphorylation by TAOK2 contributes to septin accumulation in Alzheimer's disease remains to be examined. The mouse model of 16p11.2 deletion exhibits synaptic defects, brain anatomical abnormalities, and behavioral perturbations such as hyperactivity and habituation defect (Portmann et al., 2014). It is of interest to determine whether levels of phosphorylated Sept7 are perturbed in patients and animal models with 16p11.2 deletion or duplication associated with an imbalance in TAOK2 gene dosage, and the potential impact of such alterations to the pathology of autism and schizophrenia associated with 16p11.2 CNV.

EXPERIMENTAL PROCEDURES

Neuronal Cultures and Transfection

Hippocampi were obtained from E18 Sprague-Dawley rat (Harlan Lab) embryos, trypsin dissociated, and plated at a density of 150,000 neurons per 18 mm glass coverslips (Fisher) or 450,000 neurons per 35 mm glass-bottom dish (MaTek), which were coated with 0.06 mg/mL poly-D-lysine (Sigma) and 0.0025 mg/mL laminin (Sigma). Plating media containing 10% fetal bovine serum (HyClone), 0.45% dextrose, 0.11 mg/mL sodium pyruvate, 2 mM glutamine in MEM with Earle's BBS was used, and 4 hr after seeding neurons; media was changed to maintenance media with Neurobasal Media (Invitrogen) containing B27 (Invitrogen), 100 units/mL penicillin and 100 mcg/mL streptomycin and 0.5 mM glutamine. Half of the media was replaced with new maintenance media every 3–4 days. For exogenous gene expression, neurons were transfected with 0.5–1.0 μg plasmid DNA per coverslip in a 12-well plate (or 2–3 μg DNA/35 mm dish) using Lipofectamine-2000 (Invitrogen) following manufacturer's guidelines.

Microscopy

All fixed samples were imaged on an upright Leica SP5 laser-scanning confocal microscope with a 40× or 63X NA1.4 oil objective. Images of dendritic spines were acquired as confocal stacks of 1,024 × 1,024 pixels using the 63× objective with a 6×–8× digital zoom and 0.3 micron z section. Live neuronal imaging was performed with a 60× oil objective on a Nikon Ti-E microscope equipped with Yokagawa CSU22 spinning disk confocal, an automated Peizo stage with Perfect Focus System, CO_2 and temperature-controlled OkoLab incubator, and 491 and 561 nm laser lines. Photobleaching experiments were performed on an inverted Leica SP8 laser-scanning confocal microscope using the argon 488 nm laser line.

TAOK2 Substrate Labeling

Covalent capture to identify TAOK2 kinase substrates using mass spectrometry was done as previously described (Ultanir et al., 2012, 2014) and is explained in detail in Supplemental Experimental Procedures.

Statistical Analysis

Statistical analysis was performed using the GraphPad Prism 6.0 software. For statistical significance; $p > 0.05$ is not significant (ns), $0.01 < p < 0.05$ is denoted by *, $0.001 < p < 0.01$ is denoted by **, $0.0001 < p < 0.001$ by ***, and $p < 0.0001$ is denoted by ****. Details can be found for individual experiments in the Supplemental Information or the figure legend.

SUPPLEMENTAL INFORMATION

Supplemental Information includes Supplemental Experimental Procedures, seven figures, and four movies and can be found with this article online at http://dx.doi.org/10.1016/j.neuron.2016.12.006.

AUTHOR CONTRIBUTIONS

S.Y. and Y.N.J. designed the study. All experiments and data analysis were conducted by S.Y. unless otherwise indicated. J.A.O.-P. performed the mass spectrometry and analyzed the mass-spec peak data under the

supervision of A.L.B. C.J.P. performed and analyzed the electrophysiology experiments. J.Z. performed the in utero electroporation under the supervision of S.J.P. The manuscript was written by S.Y. and all other authors, Y.N.J., J.A.O.-P., A.L.B., C.J.P., J.Z., S.J.P., and L.Y.J. provided comments and suggestions.

ACKNOWLEDGMENTS

We thank Marena Tynan-La Fontaine for slicing fixed mouse brains for imaging experiments. We thank Dr. Elliot Spiliotis, Dr. Li-Huie Tsai, Dr. Randy Hall, Dr. Thomas Südhof, and Dr. Roger Nicoll for generously providing us with plasmids. This study was supported by NIH "Pathway to Independence" grant 1K99MH108648 to S.Y. and NIH grants R37NS040929 and R37MH065334 to Y.N.J. and L.Y.J., respectively. L.Y.J. and Y.N.J. are investigators of Howard Hughes Medical Institute. Calcium imaging was performed at the Nikon Imaging Core (UCSF) using the Micro-Manager software. Mass spectrometry experiments were performed at the Biomedical Mass Spectrometry Resource at UCSF (A.L.B., Director) supported by funding from the Biomedical Technology Research Centers Program of the NIH (NIGMS 8P41GM103481) and Howard Hughes Medical Institute.

Received: March 15, 2016
Revised: October 11, 2016
Accepted: November 23, 2016
Published: January 5, 2017

REFERENCES

Adrian, M., Kusters, R., Wierenga, C.J., Storm, C., Hoogenraad, C.C., and Kapitein, L.C. (2014). Barriers in the brain: resolving dendritic spine morphology and compartmentalization. Front. Neuroanat. *8*, 142.

Ageta-Ishihara, N., Miyata, T., Ohshima, C., Watanabe, M., Sato, Y., Hamamura, Y., Higashiyama, T., Mazitschek, R., Bito, H., and Kinoshita, M. (2013). Septins promote dendrite and axon development by negatively regulating microtubule stability via HDAC6-mediated deacetylation. Nat. Commun. *4*, 2532.

Beites, C.L., Xie, H., Bowser, R., and Trimble, W.S. (1999). The septin CDCrel-1 binds syntaxin and inhibits exocytosis. Nat. Neurosci. *2*, 434–439.

Blanpied, T.A., and Ehlers, M.D. (2004). Microanatomy of dendritic spines: emerging principles of synaptic pathology in psychiatric and neurological disease. Biol. Psychiatry *55*, 1121–1127.

Caudron, F., and Barral, Y. (2009). Septins and the lateral compartmentalization of eukaryotic membranes. Dev. Cell *16*, 493–506.

Chen, Y., and Sabatini, B.L. (2012). Signaling in dendritic spines and spine microdomains. Curr. Opin. Neurobiol. *22*, 389–396.

Cho, S.-J., Lee, H., Dutta, S., Song, J., Walikonis, R., and Moon, I.S. (2011). Septin 6 regulates the cytoarchitecture of neurons through localization at dendritic branch points and bases of protrusions. Mol. Cells *32*, 89–98.

Clauser, K.R., Baker, P., and Burlingame, A.L. (1999). Role of accurate mass measurement (+/- 10 ppm) in protein identification strategies employing MS or MS/MS and database searching. Anal. Chem. *71*, 2871–2882.

Colgan, L.A., and Yasuda, R. (2014). Plasticity of dendritic spines: subcompartmentalization of signaling. Annu. Rev. Physiol. *76*, 365–385.

Darnell, J.C., Van Driesche, S.J., Zhang, C., Hung, K.Y.S., Mele, A., Fraser, C.E., Stone, E.F., Chen, C., Fak, J.J., Chi, S.W., et al. (2011). FMRP stalls ribosomal translocation on mRNAs linked to synaptic function and autism. Cell *146*, 247–261.

de Almeida Marques, I., Valadares, N.F., Garcia, W., Damalio, J.C.P., Macedo, J.N.A., de Araújo, A.P.U., Botello, C.A., Andreu, J.M., and Garratt, R.C. (2012). Septin C-terminal domain interactions: implications for filament stability and assembly. Cell Biochem. Biophys. *62*, 317–328.

de Anda, F.C., Rosario, A.L., Durak, O., Tran, T., Gräff, J., Meletis, K., Rei, D., Soda, T., Madabhushi, R., Ginty, D.D., et al. (2012). Autism spectrum disorder susceptibility gene TAOK2 affects basal dendrite formation in the neocortex. Nat. Neurosci. *15*, 1022–1031.

De Rubeis, S., He, X., Goldberg, A.P., Poultney, C.S., Samocha, K., Cicek, A.E., Kou, Y., Liu, L., Fromer, M., Walker, S., et al.; DDD Study; Homozygosity Mapping Collaborative for Autism; UK10K Consortium (2014). Synaptic, transcriptional and chromatin genes disrupted in autism. Nature *515*, 209–215.

Duman, J.G., Tzeng, C.P., Tu, Y.-K., Munjal, T., Schwechter, B., Ho, T.S.-Y., and Tolias, K.F. (2013). The adhesion-GPCR BAI1 regulates synaptogenesis by controlling the recruitment of the Par3/Tiam1 polarity complex to synaptic sites. J. Neurosci. *33*, 6964–6978.

Ewers, H., Tada, T., Petersen, J.D., Racz, B., Sheng, M., and Choquet, D. (2014). A Septin-dependent diffusion barrier at dendritic spine necks. PLoS ONE *9*, e113916.

Finnigan, G.C., Booth, E.A., Duvalyan, A., Liao, E.N., and Thorner, J. (2015). The carboxy-terminal tails of septins Cdc11 and Shs1 recruit myosin-II binding factor Bni5 to the bud neck in Saccharomyces cerevisiae. Genetics *200*, 843–862.

Gaffield, M.A., and Betz, W.J. (2006). Imaging synaptic vesicle exocytosis and endocytosis with FM dyes. Nat. Protoc. *1*, 2916–2921.

Glantz, L.A., and Lewis, D.A. (2000). Decreased dendritic spine density on prefrontal cortical pyramidal neurons in schizophrenia. Arch. Gen. Psychiatry *57*, 65–73.

Guan, S., Price, J.C., Prusiner, S.B., Ghaemmaghami, S., and Burlingame, A.L. (2011). A data processing pipeline for mammalian proteome dynamics studies using stable isotope metabolic labeling. Mol. Cell Proteomics. http://dx.doi.org/10.1074/mcp.M111.010728.

Hering, H., and Sheng, M. (2001). Dendritic spines: structure, dynamics and regulation. Nat. Rev. Neurosci. *2*, 880–888.

Hertz, N.T., Wang, B.T., Allen, J.J., Zhang, C., Dar, A.C., Burlingame, A.L., and Shokat, K.M. (2010). Chemical genetic approach for kinase-substrate mapping by covalent capture of thiophosphopeptides and analysis by mass spectrometry. Curr. Protoc. Chem. Biol. *2*, 15–36.

Holtmaat, A., and Svoboda, K. (2009). Experience-dependent structural synaptic plasticity in the mammalian brain. Nat. Rev. Neurosci. *10*, 647–658.

Hu, J., Bai, X., Bowen, J.R., Dolat, L., Korobova, F., Yu, W., Baas, P.W., Svitkina, T., Gallo, G., and Spiliotis, E.T. (2012). Septin-driven coordination of actin and microtubule remodeling regulates the collateral branching of axons. Curr. Biol. *22*, 1109–1115.

Hutsler, J.J., and Zhang, H. (2010). Increased dendritic spine densities on cortical projection neurons in autism spectrum disorders. Brain Res. *1309*, 83–94.

Ide, M., and Lewis, D.A. (2010). Altered cortical CDC42 signaling pathways in schizophrenia: implications for dendritic spine deficits. Biol. Psychiatry *68*, 25–32.

Irwin, S.A., Patel, B., Idupulapati, M., Harris, J.B., Crisostomo, R.A., Larsen, B.P., Kooy, F., Willems, P.J., Cras, P., Kozlowski, P.B., et al. (2001). Abnormal dendritic spine characteristics in the temporal and visual cortices of patients with fragile-X syndrome: a quantitative examination. Am. J. Med. Genet. *98*, 161–167.

Jain, S., Yoon, S.Y., Zhu, L., Brodbeck, J., Dai, J., Walker, D., and Huang, Y. (2012). Arf4 determines dentate gyrus-mediated pattern separation by regulating dendritic spine development. PLoS ONE *7*, e46340.

Kapfhamer, D., Taylor, S., Zou, M.E., Lim, J.P., Kharazia, V., and Heberlein, U. (2013). Taok2 controls behavioral response to ethanol in mice. Genes Brain Behav. *12*, 87–97.

Kaufmann, W.E., and Moser, H.W. (2000). Dendritic anomalies in disorders associated with mental retardation. Cereb. Cortex *10*, 981–991.

Kim, E., and Sheng, M. (2004). PDZ domain proteins of synapses. Nat. Rev. Neurosci. *5*, 771–781.

King, I., and Heberlein, U. (2011). Tao kinases as coordinators of actin and microtubule dynamics in developing neurons. Commun. Integr. Biol. *4*, 554–556.

Kopec, C.D., Li, B., Wei, W., Boehm, J., and Malinow, R. (2006). Glutamate receptor exocytosis and spine enlargement during chemically induced long-term potentiation. J. Neurosci. *26*, 2000–2009.

Kremer, B.E., Haystead, T., and Macara, I.G. (2005). Mammalian septins regulate microtubule stability through interaction with the microtubule-binding protein MAP4. Mol. Biol. Cell *16*, 4648–4659.

Kumar, R.A., KaraMohamed, S., Sudi, J., Conrad, D.F., Brune, C., Badner, J.A., Gilliam, T.C., Nowak, N.J., Cook, E.H., Jr., Dobyns, W.B., and Christian, S.L. (2008). Recurrent 16p11.2 microdeletions in autism. Hum. Mol. Genet. *17*, 628–638.

Lee, K.F.H., Soares, C., and Béïque, J.-C. (2012). Examining form and function of dendritic spines. Neural Plast. *2012*, 704103–704109.

Lin, Y.-C., and Koleske, A.J. (2010). Mechanisms of synapse and dendrite maintenance and their disruption in psychiatric and neurodegenerative disorders. Annu. Rev. Neurosci. *33*, 349–378.

Luo, R., Sanders, S.J., Tian, Y., Voineagu, I., Huang, N., Chu, S.H., Klei, L., Cai, C., Ou, J., Lowe, J.K., et al. (2012). Genome-wide transcriptome profiling reveals the functional impact of rare de novo and recurrent CNVs in autism spectrum disorders. Am. J. Hum. Genet. *91*, 38–55.

MacGillavry, H.D., and Hoogenraad, C.C. (2015). The internal architecture of dendritic spines revealed by super-resolution imaging: What did we learn so far? Exp. Cell Res. *335*, 180–186.

Maillard, A.M., Ruef, A., Pizzagalli, F., Migliavacca, E., Hippolyte, L., Adaszewski, S., Dukart, J., Ferrari, C., Conus, P., Männik, K., et al.; 16p11.2 European Consortium (2015). The 16p11.2 locus modulates brain structures common to autism, schizophrenia and obesity. Mol. Psychiatry *20*, 140–147.

Marttinen, M., Kurkinen, K.M., Soininen, H., Haapasalo, A., and Hiltunen, M. (2015). Synaptic dysfunction and septin protein family members in neurodegenerative diseases. Mol. Neurodegener. *10*, 16.

McCarthy, S.E., Makarov, V., Kirov, G., Addington, A.M., McClellan, J., Yoon, S., Perkins, D.O., Dickel, D.E., Kusenda, M., Krastoshevsky, O., et al.; Wellcome Trust Case Control Consortium (2009). Microduplications of 16p11.2 are associated with schizophrenia. Nat. Genet. *41*, 1223–1227.

Migliavacca, E., Golzio, C., Männik, K., Blumenthal, I., Oh, E.C., Harewood, L., Kosmicki, J.A., Loviglio, M.N., Giannuzzi, G., Hippolyte, L., et al.; 16p11.2 European Consortium (2015). A potential contributory role for ciliary dysfunction in the 16p11.2 600 kb BP4-BP5 pathology. Am. J. Hum. Genet. *96*, 784–796.

Moore, T.M., Garg, R., Johnson, C., Coptcoat, M.J., Ridley, A.J., and Morris, J.D. (2000). PSK, a novel STE20-like kinase derived from prostatic carcinoma that activates the c-Jun N-terminal kinase mitogen-activated protein kinase pathway and regulates actin cytoskeletal organization. J. Biol. Chem. *275*, 4311–4322.

Mostowy, S., and Cossart, P. (2012). Septins: the fourth component of the cytoskeleton. Nat. Rev. Mol. Cell Biol. *13*, 183–194.

Nimchinsky, E.A., Sabatini, B.L., and Svoboda, K. (2002). Structure and function of dendritic spines. Annu. Rev. Physiol. *64*, 313–353.

Penzes, P., Cahill, M.E., Jones, K.A., VanLeeuwen, J.-E., and Woolfrey, K.M. (2011). Dendritic spine pathology in neuropsychiatric disorders. Nat. Neurosci. *14*, 285–293.

Pinto, D., Delaby, E., Merico, D., Barbosa, M., Merikangas, A., Klei, L., Thiruvahindrapuram, B., Xu, X., Ziman, R., Wang, Z., et al. (2014). Convergence of genes and cellular pathways dysregulated in autism spectrum disorders. Am. J. Hum. Genet. *94*, 677–694.

Portmann, T., Yang, M., Mao, R., Panagiotakos, G., Ellegood, J., Dolen, G., Bader, P.L., Grueter, B.A., Goold, C., Fisher, E., et al. (2014). Behavioral abnormalities and circuit defects in the basal ganglia of a mouse model of 16p11.2 deletion syndrome. Cell Rep. *7*, 1077–1092.

Sabatini, B.L., Maravall, M., and Svoboda, K. (2001). Ca(2+) signaling in dendritic spines. Curr. Opin. Neurobiol. *11*, 349–356.

Sabatini, B.L., Oertner, T.G., and Svoboda, K. (2002). The life cycle of Ca(2+) ions in dendritic spines. Neuron *33*, 439–452.

Sala, C., and Segal, M. (2014). Dendritic spines: the locus of structural and functional plasticity. Physiol. Rev. *94*, 141–188.

Sebat, J., Lakshmi, B., Malhotra, D., Troge, J., Lese-Martin, C., Walsh, T., Yamrom, B., Yoon, S., Krasnitz, A., Kendall, J., et al. (2007). Strong association of de novo copy number mutations with autism. Science *316*, 445–449.

Sirajuddin, M., Farkasovsky, M., Hauer, F., Kühlmann, D., Macara, I.G., Weyand, M., Stark, H., and Wittinghofer, A. (2007). Structural insight into filament formation by mammalian septins. Nature *449*, 311–315.

Sturgill, J.F., Steiner, P., Czervionke, B.L., and Sabatini, B.L. (2009). Distinct domains within PSD-95 mediate synaptic incorporation, stabilization, and activity-dependent trafficking. J. Neurosci. *29*, 12845–12854.

Tada, T., Simonetta, A., Batterton, M., Kinoshita, M., Edbauer, D., and Sheng, M. (2007). Role of Septin cytoskeleton in spine morphogenesis and dendrite development in neurons. Curr. Biol. *17*, 1752–1758.

Tavares, I.A., Touma, D., Lynham, S., Troakes, C., Schober, M., Causevic, M., Garg, R., Noble, W., Killick, R., Bodi, I., et al. (2013). Prostate-derived sterile 20-like kinases (PSKs/TAOKs) phosphorylate tau protein and are activated in tangle-bearing neurons in Alzheimer disease. J. Biol. Chem. *288*, 15418–15429.

Ultanir, S.K., Hertz, N.T., Li, G., Ge, W.-P., Burlingame, A.L., Pleasure, S.J., Shokat, K.M., Jan, L.Y., and Jan, Y.-N. (2012). Chemical genetic identification of NDR1/2 kinase substrates AAK1 and Rabin8 Uncovers their roles in dendrite arborization and spine development. Neuron *73*, 1127–1142.

Ultanir, S.K., Yadav, S., Hertz, N.T., Oses-Prieto, J.A., Claxton, S., Burlingame, A.L., Shokat, K.M., Jan, L.Y., and Jan, Y.-N. (2014). MST3 kinase phosphorylates TAO1/2 to enable Myosin Va function in promoting spine synapse development. Neuron *84*, 968–982.

Weirich, C.S., Erzberger, J.P., and Barral, Y. (2008). The septin family of GTPases: architecture and dynamics. Nat. Rev. Mol. Cell Biol. *9*, 478–489.

Weiss, L.A., Shen, Y., Korn, J.M., Arking, D.E., Miller, D.T., Fossdal, R., Saemundsen, E., Stefansson, H., Ferreira, M.A.R., Green, T., et al.; Autism Consortium (2008). Association between microdeletion and microduplication at 16p11.2 and autism. N. Engl. J. Med. *358*, 667–675.

Xie, Y., Vessey, J.P., Konecna, A., Dahm, R., Macchi, P., and Kiebler, M.A. (2007). The GTP-binding protein Septin 7 is critical for dendrite branching and dendritic-spine morphology. Curr. Biol. *17*, 1746–1751.

Yasuda, S., Tanaka, H., Sugiura, H., Okamura, K., Sakaguchi, T., Tran, U., Takemiya, T., Mizoguchi, A., Yagita, Y., Sakurai, T., et al. (2007). Activity-induced protocadherin arcadlin regulates dendritic spine number by triggering N-cadherin endocytosis via TAO2beta and p38 MAP kinases. Neuron *56*, 456–471.

Yuste, R., Majewska, A., and Holthoff, K. (2000). From form to function: calcium compartmentalization in dendritic spines. Nat. Neurosci. *3*, 653–659.

Zhu, D., Li, C., Swanson, A.M., Villalba, R.M., Guo, J., Zhang, Z., Matheny, S., Murakami, T., Stephenson, J.R., Daniel, S., et al. (2015). BAI1 regulates spatial learning and synaptic plasticity in the hippocampus. J. Clin. Invest. *125*, 1497–1508.